Journal of Metals, Materials and Minerals, Vol. 33, No. 1, pp. 1-7, 2023

Wear behavior of in-situ oxide dispersion strengthened Fe-8Ni alloy with Zr additions

Mustafa TEKİN[1,*], Faiz MUHAFFEL[2], Hasan KOTAN[3], and Murat BAYDOĞAN[2]

[1] *Department of Mechatronics Engineering, KTO Karatay University, Konya 42020, Turkey*
[2] *Department of Metallurgical and Materials Engineering, Istanbul Technical University, Istanbul 34469, Turkey*
[3] *Department of Metallurgical and Materials Engineering, Konya Necmettin Erbakan University, Konya 42090, Turkey*

***Corresponding author e-mail:** mustafa.tekin@karatay.edu.tr

Received date:
19 December 2022
Revised date
9 February 2023
Accepted date:
19 February 2023

Keywords:
Oxide dispersion strengthened alloys;
Wear test;
Wear behavior;
Second precipitates

Abstract

In this study, in-situ oxide dispersion strengthened (ODS) $Fe_{91}Ni_8Zr_1$ and $Fe_{88}Ni_8Zr_4$ alloys were produced by combination of high energy mechanical alloying (HEMA) and high temperature equal channel angular extrusion (HT-ECAE). The wear behaviors of the consolidated samples were investigated under different loads from 1 N to 4 N by reciprocating wear tests at room temperature. The Scanning electron microscopy (SEM) was used to examine the wear tracks to analyze the wear characteristics as a function of applied loads. The relative comparison of the wear results showed that under the lower loads of 1 N and 2 N, $Fe_{88}Ni_8Zr_4$ alloy has lower wear rate than $Fe_{91}Ni_8Zr_1$ alloy whereas under the higher loads of 3 N and 4 N, it is vice versa. Additionally, the friction coefficient of $Fe_{91}Ni_8Zr_1$ alloy was found to be lower than that of $Fe_{88}Ni_8Zr_4$ alloy under all the applied loads. The results were comparatively discussed with respect to microstructural features of 1 at% Zr and 4 at% Zr containing ODS alloys produced by HEMA followed by ECAE. The obtained results of ODS alloys with different grain size, precipitate size, and number density of the precipitates, may disclose a new sight for using such alloys in wear applications just as cutting tools, turbine blades, and discs.

1. Introduction

Fe-based Oxide Dispersion Strengthened (ODS) alloys with stabilized microstructures have been considered for the advanced structural applications such as future nuclear reactors due to their excellent strength, fatigue and creep properties and high resistance to irradiation as well as thermomechanical stability [1-5]. The design and synthesis of Fe-based alloys with nano-sized precipitates or clusters homogeneously distributed in the matrix using high energy mechanical alloying (HEMA) is one of the effective avenues to develop the required microstructural features for such applications [6]. Over the past decade, Fe-Ni and Fe-Cr alloys with Zr additions have captured great attention due to their high temperature micro-structural stability and enhanced mechanical properties. Synthesis of Fe-Ni-Zr alloys via HEMA followed by either conventional sintering [7,8] or high temperature equal channel angular extrusion (HT-ECAE) [9-11] resulted in precipitation of Zr-based intermetallics and oxide based clusters homogeneously distributed in the microstructure. Forming of precipitates and clusters have been reported to contribute to grain size stability and increased mechanical properties under the extreme conditions, i.e., high temperature compression tests in the same studies. That is, depending on the type, amount, and size of the in situ formed second phases, grain size stabilization through Zener pinning [12-15] and strengthening through Orowan mechanism [16] can be achieved and tailored for the needs required for specific applications.

The microstructural characterizations of Fe-Ni-Zr alloys after HEMA and consolidation via HT-ECAE were conducted previously by Barton *et al*. [9] and Darling *et al*. [10] in detail using Transmission electron microscopy (TEM), Scanning transmission electron microscopy (STEM), and atom probe tomography (APT). The results showed that HT-ECAE of mechanically alloyed nanocrystalline Fe-Ni-Zr powders produced different microstructures resulted from varying Zr content and consolidation temperature. That is, different microstructures with a range of grain size, precipitate size, and number density of the precipitates were achieved, which in turns altered the mechanical properties. For example, after ECAE consolidation at 1000°C, the grain sizes were reported as around 4 μm for $Fe_{91}Ni_8Zr_1$ alloy and 5 μm for $Fe_{91}Ni_8Zr_4$ alloy with the Zr based oxide clusters smaller than 10 nm as well as larger precipitates. The number densities of clusters were also reported to be 24.2×10^{22} m^{-3} and 3.51×10^{22} m^{-3} for $Fe_{91}Ni_8Zr_1$ and $Fe_{91}Ni_8Zr_4$ alloys, respectively [9,10].

The mechanical properties of these alloys obtained through hardness and compressive tests both at room and high temperatures were also discussed and linked to the microstructure, Zr content, and processing conditions [11]. It was reported that even though grain growth to micron sizes occurred in Fe-Ni-Zr alloys after ECAE consolidation at high temperatures, the Zr-based clusters and complex oxide phases formed during processing inducing Orowan strengthening effect rivaling that predicted by the Hall–Petch strengthening for the smallest grain size of the same alloys. Accordingly, Zr addition to Fe-Ni alloys led to increased hardness (~6 GPa) compared to pure Fe (~2 GPa) and Fe-Ni (~2.8 GPa) after conventional annealing at 1000°C [17]. The room temperature compressive yield strengths of Fe-8Ni alloys with 1 and 4 at% Zr were reported as 1050 MPa and 1080 MPa, respectively, after HT-ECAE at 1000°C [11]. Additionally, increasing compressive testing temperature to 600°C reduced the yield

strengths down to only around 350 MPa to 400 MPa for $Fe_{91}Ni_8Zr_1$ alloy and 550 MPa to 600 MPa for $Fe_{91}Ni_8Zr_4$ alloy as reported in [11].

In conclusion, the reported results regarding to microstructural evolution and mechanical properties of Fe-Ni-Zr alloys have showed that a relatively simple processing route can be used to produce exceptional mechanical properties both at room temperature and at elevated temperatures. Although various mechanical tests were conducted for HT-ECAE of Fe-Ni-Zr alloys as referenced above, the wear behaviors of these materials have not been investigated yet. The tribological behavior of steels has critical importance due to potential usage in a wide range of applications such as fabrication discs, pump bodies and components, nuclear reactor parts, fuel cladding applications, and hot extrusion tools [18]. Therefore, several studies in the literature examined the wear behavior of steels from various points of view: temperature, normal load, sliding distance, grain size, and hardness [19,20]. It is also known that small second phases and/or clusters are expected to increase the wear resistance [11,12]. Thus, the aim of the present work is to investigate the effect of precipitates on the wear behavior of Fe-Ni-Zr alloys by reciprocating wear tests to promote the use of such alloys over a wider range of industrial applications.

2. Experimental procedures

$Fe_{91}Ni_8Zr_1$ and $Fe_{88}Ni_8Zr_4$ (at%) alloys, which will be referred as 1Zr alloy and 4Zr alloy throughout this paper, respectively, were produced by HEMA followed by HT-ECAE. The appropriate amounts of Fe, Ni, and Zr with a total weight of 10 g were loaded in hardened steel vials along with milling media under an Ar atmosphere before milling. Room temperature mechanical milling was carried out with a 10:1 ball to powder ratio for 20 h. After the milling, the as-milled powders were held in the glove box until the required amount of powder was generated for the consolidation process via extrusion. Prior to the HT-ECAE process, the die assembly was heated to about 300°C. The nickel can was loaded with mechanically alloyed powders, which was equilibrated for 30 min in a box furnace under protective Ar gas atmosphere at 1000°C. Following the quick removal of the nickel can from the box furnace, consolidation process with ECAE was performed and repeated four times using $4B_c$ processing route. The details of the experimental procedures for HEMA and subsequent HT-ECAE processes are reported in [9,10]. A part of the extruded samples was serial sectioned with a thickness of 0.6 mm using wire electric discharge machining for the wear tests. Figure 1 shows the schematic illustrations of HEMA and HT-ECAE processes.

Reciprocating wear tests were performed according to ASTM standard G133, against an alumina ball (purity 99.80%, Ra: 0.02 µm, 18.6 GPa) of 6 mm in diameter as the counter body, sliding backward and forward on the samples with a sliding speed of 6 $mm \cdot s^{-1}$. Sliding amplitude and the total sliding distance were 2 mm and 30 m, respectively. Loads applied to the specimens during the wear tests were 1 N, 2 N, 3 N, and 4 N. Following the wear tests, dimensions of the wear tracks were measured to calculate the wear area by a surface profilometer, which is a semi-manual machine that presents the profile data of the samples with the vertical detection system by moving stylus on the surface. Measurement of the wear tracks were repeated three times along the wear track, and the averaged values were used the wear rate.

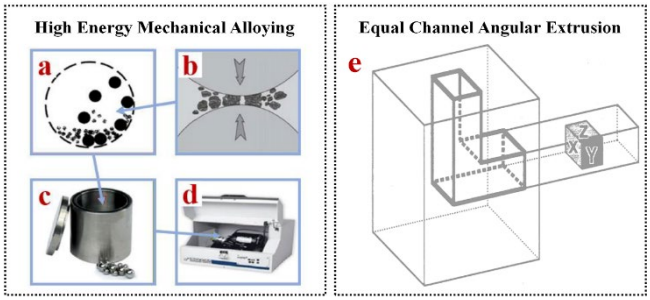

Figure 1. Schematic illustration of high energy mechanical alloying [21], (a) ball-powder interaction during milling, (b) ball-to-powder interaction, (c) milling media, vial, and balls, (d) SPEX 8000 mill and (e) equal channel angular extrusion [22].

Wear rates of the alloys with respect to test loads were determined using Equation (1) [23] normalizing the worn volume with applied load and sliding distance. Worn volumes of the alloys were also calculated with multiplication of the area and amplitude of the wear tracks.

$$V_i = k_i.F.s \quad (1)$$

where F is the normal load, s is the sliding distance, V_i is the wear volume and k_i is the specific wear rate coefficient. Index i identifies the tested surface.

Wear tracks were also examined by a scanning electron microscopy (SEM) to investigate the wear characteristics. Conventional micro-hardness tests were also carried out to examine the influence of Zr content on the hardness with a load of 10 g and a dwell time of 10 s.

3. Experimental results

Figure 2 shows that the wear rates of both alloys vary in between 0.05 to 0.35 ($\times 10^{-13}$ $m^3 \cdot Nm^{-1}$) suggesting that the applied test loads resulted in different wear characteristics depending on the Zr content. For example, the increased applied load from 1 N to 4 N does not result in a significant change in wear rate for 1Zr alloy. However, wear rate of 4Zr alloy continuously increased with increasing test loads. As a result, 4Zr alloy has lower wear rate (i.e., better wear resistance) under lower loads of 1 N and 2 N, and 1Zr alloy has lower wear rate under higher loads of 3 N and 4 N.

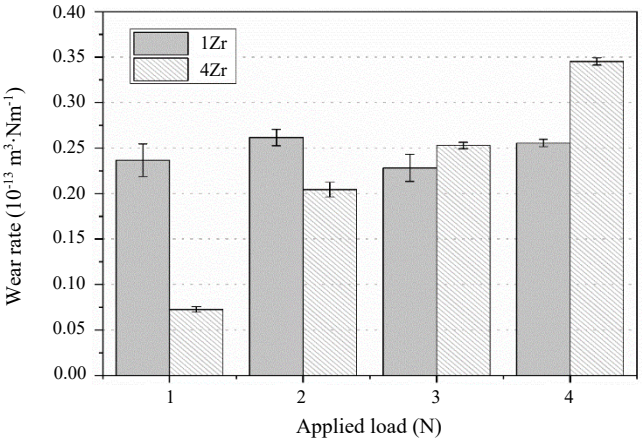

Figure 2. Wear rates of the alloys with respect the test loads.

Figure 3 reveals the influence of applied load on the mean steady-state friction coefficient for both alloys after wear tests at room temperature. It is seen that the mean steady state friction coefficient of 1Zr alloy slightly increases from 0.44 to 0.46 and reaches to a maximum value at 2 N, then decreases with increasing test load.

By contrast, for 4Zr alloy, the mean steady state friction coefficient decreases noticeably at 2 N and reaches to value around 0.52 when the load is increased to 3 N, then followed by a decrement at 4 N applied test load. It is worth noting that the mean steady state friction coefficients of 4Zr alloys are always higher than that of 1Zr alloy.

Figure 4(a-b) illustrates the two-dimensional profiles of the wear tracks for 1Zr and 4Zr alloys as a function of applied test loads. Deeper and wider wear tracks can be seen from the Figure 4 with increasing test loads leading to larger wear track areas for both compositions. Additionally, the width and depth of the wear track of 1Zr alloy appears to be larger than those of 4Zr alloy at lower loads (1 N and 2 N), whereas it is vice versa when the load is increased to 3 N and 4N. This suggests that 4Zr alloy has better wear resistance at lower loads (1 N and 2 N) while 1Zr alloy is more resistant to wear at higher loads (3 N and 4 N).

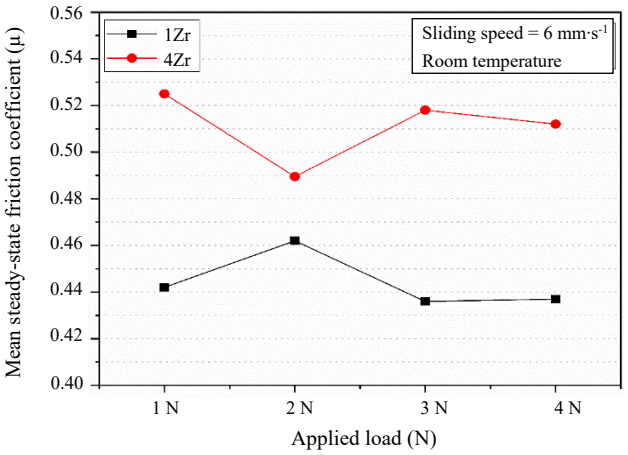

Figure 3. Influence of applied load on mean steady-state friction coefficient of 1Zr and 4Zr alloys.

Figure 5 illustrates the friction coefficient of both alloys with sliding distance at varying loads. The initial sharp rise observed in both alloys may be resulted from the initial roughness of the wear surfaces. After the initial surface roughness diminished and the surface became smoother, friction coefficient dropped, a continuous and steady increment until the end of the test were observed for both alloys.

Additionally, the friction coefficient of 4Zr alloy appears to be always higher than that of 1Zr alloy for the applied loads, as seen from Figure 5. It is well known that friction coefficient is directly associated with the applied loads and mechanical properties of the materials [18]. The hardness of the powders after HEMA, before the HT-ECAE process, were determined and reported to be around 10 GPa due to the nanocrystalline grain sizes of alloys [11]. Later, the hardness tests on the HT-ECAE consolidated samples in this study reveal that 1Zr and 4Zr alloys have hardness around 2.9 GPa and 3.3 GPa, respectively. Thus, there is a good agreement for 4Zr alloy having higher friction coefficient (COF) with higher hardness when compared to 1Zr alloy. Additionally, Figure 5(c-d) shows that the increased normal load to 3 N and 4 N does not induce any discernable changes in the variation of friction coefficient for both alloys. They show similar variation with respect to sliding distance which increases steadily until the end of the tests. Finally, as seen from Figure 5 that 1Zr alloy shows more stable values varying in a narrower band when compared to 4Zr alloy for all normal loads.

Figure 6 shows SEM wear track morphologies of 1Zr Figure 6(a-d) and 4Zr samples Figure 6(e-h) as a function of the applied test loads. At a normal load of 1N, the wear track of 1Zr alloy appears to be relatively uniform with shallow scratches. The low amount of wear debris in the form of particles at the surface of 1Zr alloy indicates that the wear is progressed by uniformly removing the material from the surface. At a normal load of 2 N, wear debris begins to form and its amount increased with increasing test load to 3 N. However, there is no significant change in the size of the wear scratches. At the highest test load of 4 N, wider and deeper scratches exist in addition to more wear debris in the form of particles. Wear tracks of 4Zr alloy generally consist of wear debris in the form of isolated patches which contain some particulate material.

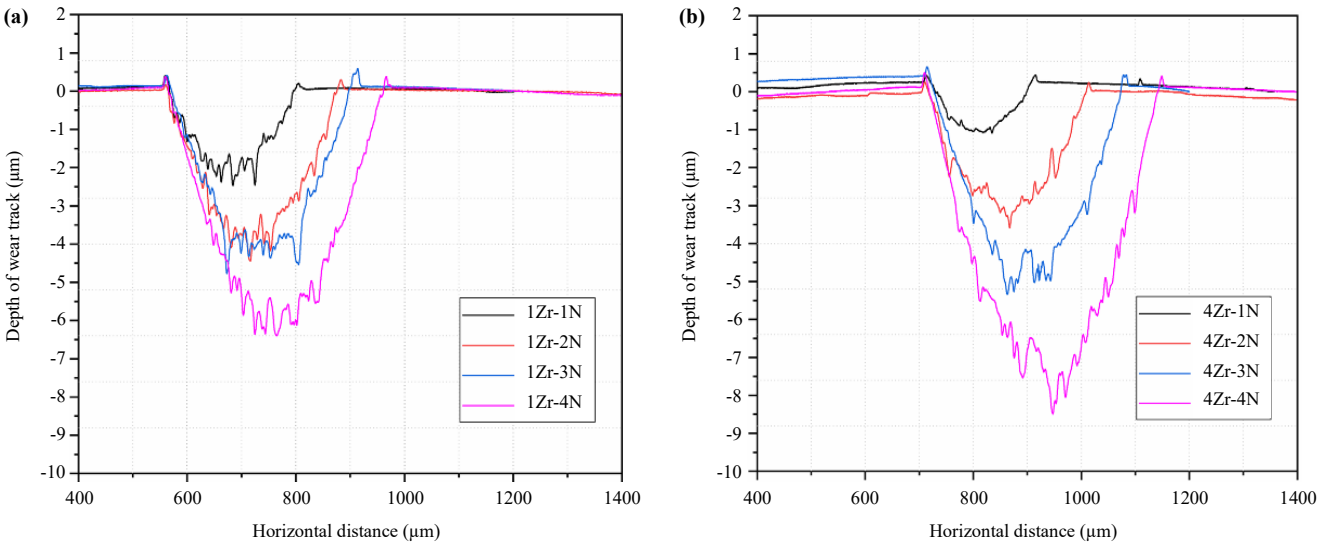

Figure 4. Two dimensional profiles of the wear tracks of (a) 1Zr and (b) 4Zr containing samples.

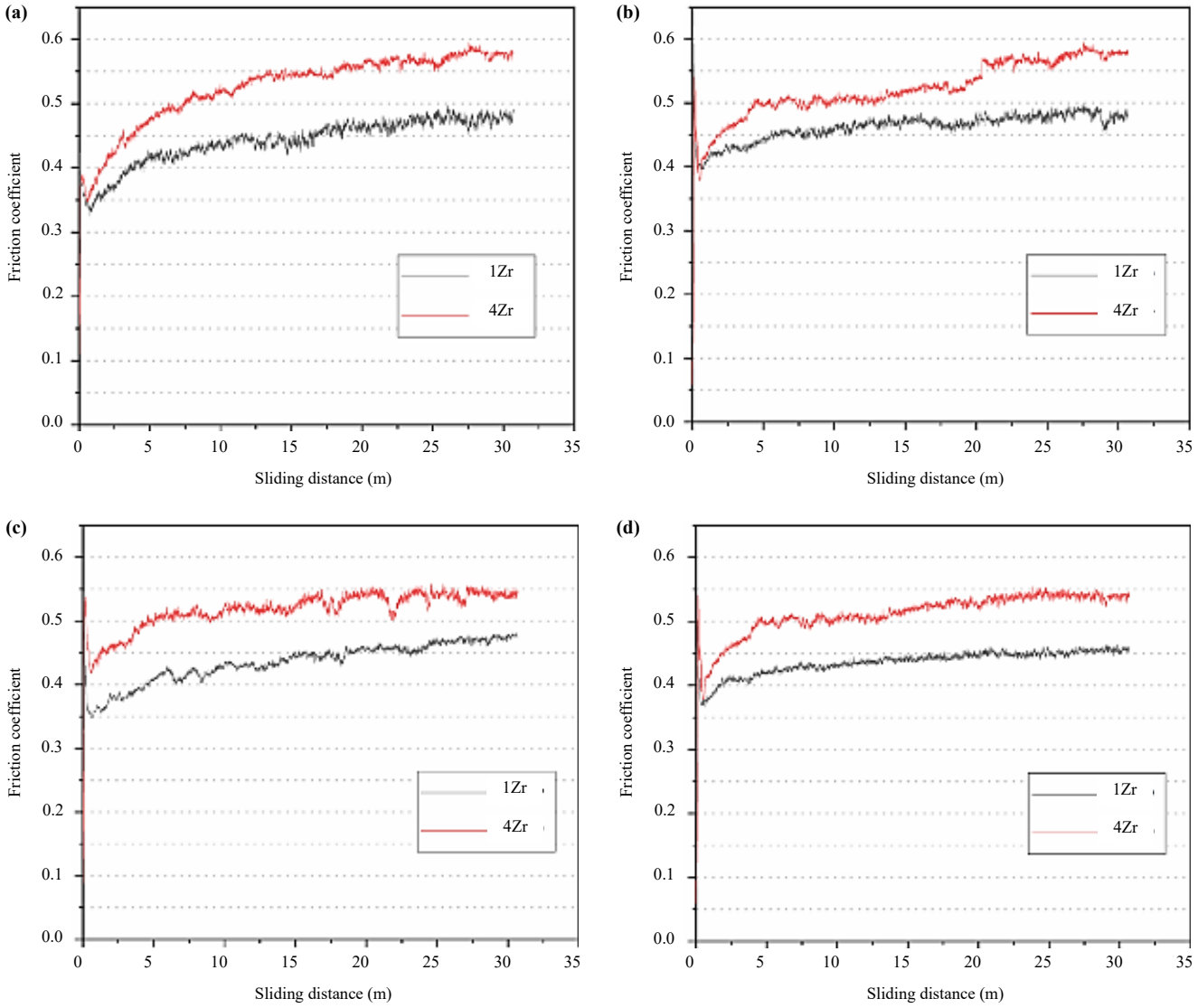

Figure 5. Variation of friction coefficient of both alloys with sliding distance at the loads of (a) 1 N, (b) 2 N, (c) 3 N, and (d) 4 N.

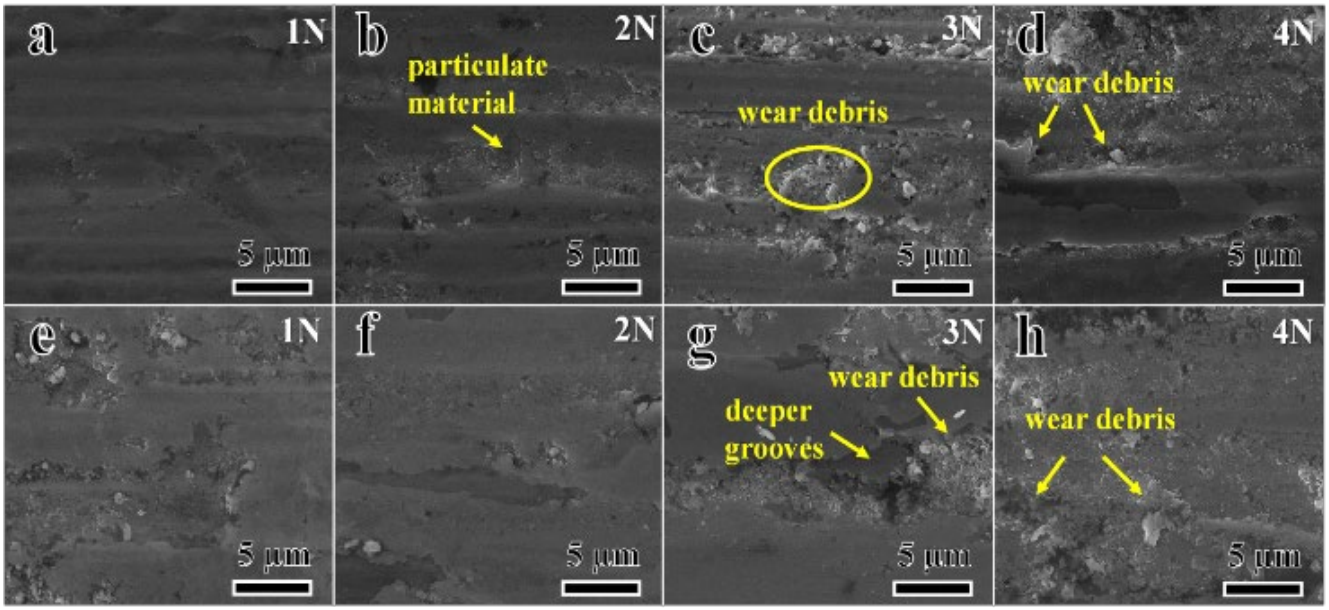

Figure 6. SEM micrographs of the wear tracks; (a-d) 1Zr alloy, and (e-h) 4Zr alloy.

In contrast to 1Zr alloy, less uniformly worn areas are observed for 4Zr alloy from at the lowest normal load (1 N). Increasing the normal load to 2 N causes almost similar wear track morphology as for 1 N.

Further increment of the normal load to 3 N and 4 N increases the surface detachments in the form of deeper grooves. At the highest normal load of 4 N, the worn surface is almost completely covered with wear debris because of the detachment of the surface materials. Thus, abrasive wear mechanism is the dominant wear characteristic for 4Zr alloy at increased test loads due to the formation of deeper groves in addition to wear debris.

4. Discussion

The results have shown that the wear characteristics of the investigated alloys are dissimilar with respect to Zr content and the applied test loads. The previously conducted detailed microstructural characterization of HT-ECAE consolidated Fe-Ni-Zr alloys by facilitating the transmission electron microscopy and atom probe tomography showed that Fe-8Ni alloys possess different precipitated second phases depending on the Zr content with different sizes and number densities [7,9,10]. That is, upon HT- ECAE consolidation at 1000°C, the kinetics of atomic diffusion became faster in the microstructure promoting the formation of complex oxide phases and nano-sized clusters in Fe-Ni-Zr based alloys.

The FIB-CCI images of 1Zr and 4Zr alloys as well as oxide precipitates with APT reconstructions of 4Zr alloy after ECAE consolidation at 1000°C are shown in Figure 7. Higher amount of secondary phases, resulted from increased Zr content, can be distinctly observed from Figure 7 (a versus b). Additionally, the size and distribution of particularly Zr-based oxide precipitates can be seen from Figure 7(c) which is considered to be responsible for the enhanced mechanical properties.

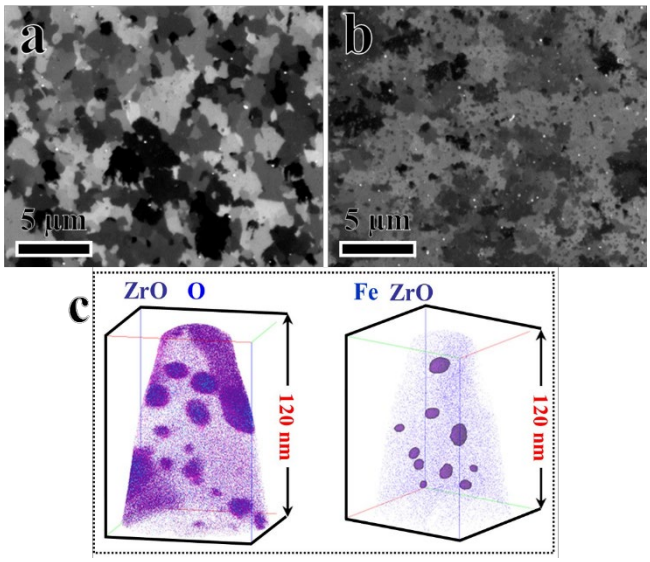

Figure 7. After ECAE consolidation at 1000°C, the FIB micrographs of (a) 1Zr, (b) 4Zr alloys, and (c) 3D atom probe tomography reconstruction of 4Zr alloy showing oxide precipitates. The FIB images are taken from Ref [11] with the permission of Springer Nature publishing and the APT reconstruction in (c) is reproduced from Ref [10] with the permission of Elsevier publishing.

The formation of those precipitates occurs due to the presence of intrinsic impurities which may come from the processing during milling and ECAE processing. Nevertheless, oxide-based clusters as small as few nm in diameter and larger precipitates composed of Fe-Ni-Zr-O were reported previously in 1Zr and 4Zr, the latter was reported mostly in the alloys with higher amount of Zr added steel i.e., 4Zr. A later study conducted by Chen *et al*. [24] investigated the effect of Zr on the grain size stability of pure Fe and confirmed the formation of Zr-O based clusters formed during processing in the microstructure which were also coherent with the matrix. In the present study, 4Zr alloy is expected to have higher amount of secondary precipitates giving that it has more Zr. Thus, it can be summarized based on the reported microstructural investigations [7,9,10] that 4Zr alloy has more but larger Fe-Ni-Zr-O precipitates in the microstructure while 1Zr alloy has much smaller clusters in the microstructure that are coherent with the matrix.

The effect of both ex-situ added and in-situ formed second phases on the wear behavior of metallic materials has been investigated and reported that the second phases in the microstructure increase wear resistance in varying range depending on the characteristics of the such phases [25-30]. It is well-known that higher amount of precipitates in the nanometer scale is very effective in hindering the dislocation movement leading to improved strength and considered to be the main reason of strengthening mechanism for the investigated alloys based on the Orowan strengthening [31,32]. As given above, under the lower loads (1 N to 2 N), 4Zr alloy shows better wear resistance (Figure 2) which is correlated with the depth of wear tracks shown in Figure 4. This could be associated with higher amount of secondary precipitates and larger Fe-Ni-Zr-O second phases in the 4Zr alloy. When the applied load was increased to 3 N to 4 N, higher Zr containing alloy tend to have worse wear resistance with more surface detachments (wear debris and deeper grooves) as illustrated in Figure 6(c-d). As reported previously [10], while the total amount of precipitates is higher for 4Zr alloy, which controls the mechanical properties such as hardness, the number density of the oxide precipitates coherent with the matrix is higher in the microstructure of 1Zr alloy with the value of 24×10^{22} m^{-3}. Such features are considered to have a positive impact on the enhanced wear resistance of 1Zr alloy [33]. That is, when the wear load is increased, secondary oxide precipitates which are coherent with the matrix for 1Zr alloy primarily begin to influence the wear characteristic and so, increase the wear resistance. Thus, it can be pointed out that increasing test loads (1 N to 4 N) for 1Zr alloy was insignificantly on the wear due to the containing these types of coherent secondary precipitates with the matrix in contrast to 4Zr alloy. It was reported that the maximizing the nano-sized particles within the grains and minimizing the volume fraction and size of the precipitates at the grain boundaries increase the wear resistance [34,35]. It is expected that the increased Zr content for 4Zr alloy results in higher secondary precipitates at the grain boundaries due to the heterogeneous nucleation weakening the wear characteristic of 4Zr alloy under the increased test loads. Additionally, a crack may occur in the ductile matrix due to the brittle secondary intermetallic phases as a result of increasing local stresses around the slip lines in the matrix [36]. Thus, higher amount of precipitates in 4Zr alloy with higher hardness (i.e., Zr rich precipitates in our alloys are 10 times

harder than the Fe rich matrix) [37] is expected to weaken the wear behavior because of the increased crack initiation in the matrix when compared to 1Zr alloy under the increased loading conditions as compared to lower loads.

5. Summary and conclusions

This study was conducted to investigate the effect of Zr addition on the wear properties of Fe-Ni-Zr alloys produced by a combination of mechanical allaying and equal channel angular extrusion. To sum up, increasing test loads from 1 N to 4 N was insignificantly for 1Zr alloy due to the containing higher amount of secondary oxide precipitates which are coherent with the matrix. On the other hand, wear behavior of 4Zr alloy has inversely affected (weakened) by the increment of test loads by means of higher total amount of secondary precipitates at the grain boundaries due to the heterogeneous nucleation and higher total amount of precipitates with higher hardness (i.e., Zr rich precipitates in our alloys are 10 times harder than the Fe rich matrix). Additionally, the following conclusions were obtained:

1. The wear rates of 1Zr alloy are 0.233 and 0.255 ($\times 10^{-13}$ $m^3 \cdot Nm^{-1}$) for 1 N and 4 N applied test loads, while the wear rates of 4Zr alloy are 0.072 and 0.345 ($\times 10^{-13}$ $m^3 \cdot Nm^{-1}$) under the same conditions.
2. Wear rate of 4Zr alloy is load dependent and increases with increasing normal load.
3. Under lower loads (1 N and 2 N), 4Zr alloy exhibits better wear resistance (lower wear rate) while 1Zr alloy has better wear resistance when the test load is increased to 3 N and 4 N. These results suggest that the higher Zr content at lower loads is beneficial when enhancing the wear resistance, and large amount of total brittle intermetallic adversely affect the wear resistance at higher loads.
4. Friction coefficient of 4Zr alloy is higher than that of 1Zr alloy under the applied loads from 1 N to 4 N.
5. The damage surfaces of the alloys indicate that less uniformly worn areas for 4Zr alloy than 1Zr alloy observed under lower loads, whereas the worn surface is almost completely covered with wear debris because of the detachment of the surface materials for 4Zr alloy at increased test loads (4N). Thus, abrasive wear mechanism is the dominant wear characteristics for 4Zr alloy under higher test loads.

Acknowledgements

The authors thank to Kris A. Darling for the support in Equal Channel Angular Extrusion (ECAE) process of alloys.

References

[1] S. Ukai, and M. Fujiwara, "Perspective of ODS alloys application in nuclear environments," *Journal of Nuclear Materials*, vol. 307, pp. 749-757, 2002.

[2] D. A. McClintock, M. A. Sokolov, D. T. Hoelzer, and R. K. Nanstad, "Mechanical properties of irradiated ODS-EUROFER and nanocluster strengthened 14YWT," *Journal of Nuclear Materials*, vol. 392, no. 2, pp. 353-359, 2009.

[3] H. Xu, Z. Lu, C. Jia, D. Feng, and C. Liu, "Influence of mechanical alloying time on morphology and properties of 15Cr-ODS steel powders," *High Temperature Materials and Processes*, vol. 35, no. 5, pp. 473-477, 2016.

[4] H. Xu, Z. Lu, C. Jia, H. Gao, and C. Liu, "Microstructure and mechanical property of 12Cr oxide dispersion strengthened steel," *High Temperature Materials and Processes*, vol. 35, no. 3, pp. 321-325, 2016.

[5] W. Li, H. Xu, X. Sha, J. Meng, and Z. Wang, "Microstructure and mechanical properties of 14Cr-ODS steels with Zr addition," *High Temperature Materials and Processes*, vol. 38, no. 2019, pp. 404-410, 2019.

[6] C. Suryanarayana, "Mechanical alloying and milling," *Progress in materials science*, vol. 46, no. 1-2, pp. 1-184, 2001.

[7] H. Kotan, and K. A. Darling, "Isothermal annealing of a thermally stabilized Fe-based ferritic alloy," *Journal of Materials Engineering and Performance*, vol. 24, no. 9, pp. 3271-3276, 2015.

[8] G. POLAT, A. B. Batibay, and H. Kotan, "Understanding microstructural evolution and hardness of nanostructured Fe_{89}. $5Ni_8Zr_2$. 5 alloy produced by mechanical alloying and pressureless sintering," *Engineering Science and Technology, an International Journal*, vol. 23, no. 5, pp. 1279-1284, 2020.

[9] D. J. Barton, C. Kale, B. C. Hornbuckle, K. A. Darling, K. N. Solanki, and G. B. Thompson, "Microstructure and dynamic strain aging behavior in oxide dispersion strengthened 91Fe-8Ni-1Zr (at%) alloy," *Materials Science and Engineering: A*, vol. 725, pp. 503-509, 2018.

[10] K. A Darling, M. Kapoor, H. Kotan, B. C. Hornbuckle, S. D. Walck, G. B. Thompson, M. A. Tschopp, and L. J. Kecskes, "Structure and mechanical properties of Fe–Ni–Zr oxide-dispersion-strengthened (ODS) alloys," Journal of Nuclear Materials, vol. 467, pp. 205-213, 2015.

[11] H. Kotan, K. A. Darling, and T. Luckenbaugh, "High temperature mechanical properties and microstructures of thermally stabilized Fe-based alloys synthesized by mechanical alloying followed by hot extrusion," Metals and Materials International, pp. 1-8, 2019.

[12] M. Hillert, "On the theory of normal and abnormal grain growth," *Acta metallurgica*, vol. 13, no. 3, pp. 227-238, 1965.

[13] T. Gladman, "On the theory of the effect of precipitate particles on grain growth in metals," *Proceedings of the Royal Society of London. Series A. Mathematical and Physical Sciences*, vol. 294, no. 1438, pp. 298-309, 1966.

[14] F. J. Humphreys, and M. Hatherly, Recrystallization and related annealing phenomena. *Elsevier*, 2012.

[15] N. Nabiran, S. Weber, and W. Theisen, "Ferritic stainless steels for high-temperature applications: stabilization of the microstructure by solid state precipitation of MX carbonitrides," *High Temperature Materials and Processes*, vol. 32, no. 6, pp. 563-572, 2013.

[16] W. A. Story, D. J. Barton, B. C. Hornbuckle, K. A. Darling, G. B. Thompson, and L. N. Brewer, "Laser assisted cold spray of Fe–Ni–Zr oxide dispersion strengthened steel," *Materialia*, vol. 3, pp. 239-242, 2018.

[17] H. Kotan, K. A. Darling, M. Saber, C. C. Koch, and R. O. Scattergood, "Effect of zirconium on grain growth and mechanical properties of a ball-milled nanocrystalline FeNi alloy," *Journal of alloys and compounds,* vol. 551, pp. 621-629, 2013.

[18] S. Karak, C. Vishnu, Z. Witczak, W. Lojkowski, J. D. Majumdar, and I. Manna, "Studies on wear behavior of nano-Y_2O_3 dispersed ferritic steel developed by mechanical alloying and hot isostatic pressing," *Wear*, vol. 270, no. 1-2, pp. 5-11, 2010.

[19] R. Autay, M. Kchaou, and F. Dammak, "Friction and wear behavior of steels under different reciprocating sliding conditions," *Tribology Transactions*, vol. 55, no. 5, pp. 590-598, 2012.

[20] A. Jourani, and S. Bouvier, "Friction and wear mechanisms of 316L stainless steel in dry sliding contact: Effect of abrasive particle size," *Tribology Transactions,* vol. 58, no. 1, pp. 131-139, 2015.

[21] H. Kotan, "Thermal stabilization and mechanical properties of nanocrystalline iron-nickel-zirconium alloys," *North Carolina State University*, 2013.

[22] J. Macheret, G. Korth, T. Lillo, A. Watkins, D. Herling, and M. Smith, "Equal channel angular extrusion," *Idaho National Engineering and Environmental Laboratory Idaho Falls, Idaho,* vol. 83415, p. 1, 1999.

[23] J. Archard, "Contact and rubbing of flat surfaces," *Journal of Applied Physic*s, vol. 24, no. 8, pp. 981-988, 1953.

[24] Y. Z. Chen, K. Wang, G. B. Shan, A. V. Ceguerra, L. K. Huang, H. Dong, L. F. Cao, S. P. Ringer, and F. Liu, "Grain size stabilization of mechanically alloyed nanocrystalline Fe-Zr alloys by forming highly dispersed coherent Fe-Zr-O nanoclusters," *Acta Materialia*, vol. 158, pp. 340-353, 2018.

[25] T. Torgerson, S. Mantri, R. Banerjee, and T. Scharf, "Room and elevated temperature sliding wear behavior and mechanisms of additively manufactured novel precipitation strengthened metallic composites," *Wear*, vol. 426, pp. 942-951, 2019.

[26] G. Pantazopoulos, T. Papazoglou, P. Psyllaki, G. Sfantos, S. Antoniou, K. Papadimitriou, and J. Sideris, "Sliding wear behaviour of a liquid nitrocarburised precipitation-hardening (PH) stainless steel," *Surface and Coatings Technology*, vol. 187, no. 1, pp. 77-85, 2004.

[27] M.-H. Chuang, M.-H. Tsai, W.-R. Wang, S.-J. Lin, and J.-W. Yeh, "Microstructure and wear behavior of AlxCo1. 5CrFeNi1. 5Tiy high-entropy alloys," *Acta Materialia*, vol. 59, no. 16, pp. 6308-6317, 2011.

[28] K. M. Asl, A. Masoudi, and F. Khomamizadeh, "The effect of different rare earth elements content on microstructure, mechanical and wear behavior of Mg–Al–Zn alloy," *Materials Science and Engineering: A*, vol. 527, no. 7-8, pp. 2027-2035, 2010.

[29] A. Martín, J. Rodríguez, and J. Llorca, "Temperature effects on the wear behavior of particulate reinforced Al-based composites," *Wear*, vol. 225, pp. 615-620, 1999.

[30] A. M. Hassan, M. Almomani, T. Qasim, and A. Ghaithan, "Effect of processing parameters on friction stir welded aluminum matrix composites wear behavior," *Materials and Manufacturing Processes*, vol. 27, no. 12, pp. 1419-1423, 2012.

[31] J. Moon, S. Kim, J.-i. Jang, J. Lee, and C. Lee, "Orowan strengthening effect on the nanoindentation hardness of the ferrite matrix in microalloyed steels," *Materials Science and Engineering: A*, vol. 487, no. 1-2, pp. 552-557, 2008.

[32] W. Zhai, W. Zhou, and S. M. L. Nai, "Grain refinement and strengthening of 316L stainless steel through addition of TiC nanoparticles and selective laser melting," *Materials Science and Engineering: A*, vol. 832, p. 142460, 2022.

[33] B. Kim, J. C. Jiang, and P. B. Aswath, "Mechanism of wear at extreme load and boundary conditions with ashless anti-wear additives: Analysis of wear surfaces and wear debris," *Wear*, vol. 270, no. 3-4, pp. 181-194, 2011.

[34] A. Mukhopadhyay, and R. I. Todd, "Relationship between microstructure and abrasive wear resistance of Al_2O_3–$FeAl_2O_4$ nanocomposites produced via solid-state precipitation," *Journal of the European Ceramic Society*, vol. 31, no. 3, pp. 339-350, 2011.

[35] W. Xi, B. Song, Z. Sun, T. Yu, J. Wang, and Q. Sun, "Effect of various morphology of in situ generated NbC particles on the wear resistance of Fe-based cladding," *Ceramics International*, 2022.

[36] J. Barnby, "The initiation of ductile failure by fractured carbides in an austenitic stainless steel," *Acta Metallurgica*, vol. 15, no. 5, pp. 903-909, 1967.

[37] N. Das, P. Sengupta, S. Roychowdhury, G Sharma, P. S. Gawde, A. Arya, V. Kain, U. D. Kulkarni, J. K. Chakravartty, G. K. Dey, "Metallurgical characterizations of Fe–Cr–Ni–Zr base alloys developed for geological disposal of radioactive hulls," *Journal of nuclear materials*, vol. 420, no. 1-3, pp. 559-574, 2012.